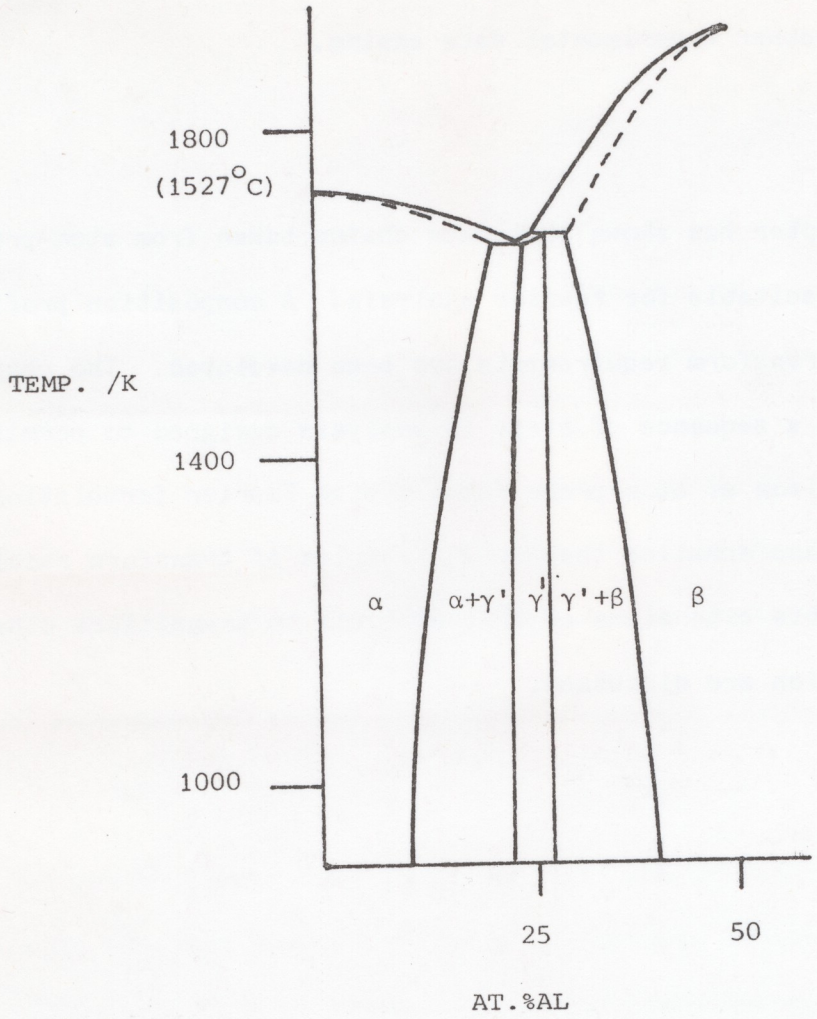

Figure 4.1 The nickel-rich end of the nickel-aluminium phase diagram (after Hansen and Anderko 1958).

CHAPTER 4

DECOMPOSITION OF SUPERSATURATED Ni-14·1at%Al SOLID SOLUTION

4.1 Constitution

The phase diagram for the nickel-rich end of the binary nickel-aluminium system is shown in figure 4.1 (after Hansen and Anderko 1958). Two phases, γ and $L1_2$, ordered γ', are present. Incoherent solubility data for γ' in nickel-aluminium matrix have been provided by e.g. Taylor and Floyd 1952a and equivalent coherent measurements by e.g. Rastogi and Ardell 1969.

4.2 Phase Transitions

4.2.1 Phase Separation

Observations supporting both continuous decomposition and conventional nucleation-plus-growth mechanisms for separation of γ' phase have been reported. Evidence for spinodal change at high solute supersaturation has been presented by Gentry and Fine 1972 (magnetization measurements) and Corey, Rosenblum and Green 1973 (TEM). Earlier observations of X-ray sidebands similar to those of modulated Cu-Ni-Fe had previously suggested this mechanism (e.g. Bagariatskii and Tyapkin 1957, 1960; Manenc 1957a,b, 1959).

Homogeneous nucleation was first suggested by Williams 1959 (TEM, resistivity, etc.). Direct observations of precipitation by TEM have subsequently confirmed the nucleation mechanism at low supersaturations e.g. Ardell, Nicholson and Eshelby 1966; Phillips 1966; Kirkwood 1970; West and Kirkwood 1976; Hirata and Kirkwood 1977. FIM work of Faulkner and Ralph 1972 again suggested nucleation. With

respect to morphology it is generally accepted that the precipitating γ' phase adopts cuboidal morphology e.g. Phillips 1966, although Faulkner and Ralph 1972 have reported spherical particles of diameter less than 10nm.

Some observations of heterogeneous nucleation have also been reported. Phillips (1966) observed precipitation only at dislocations and inclusions at considerably raised temperature (800°C). Williams (1959) presented evidence of cellular reaction at a grain boundary.

4.2.2 The Order-disorder Reaction

The long range order (LRO) transition temperature was measured by Corey and Lisowsky 1967 as 1250°C. In later work Pope and Garin 1977 confirmed LRO in the temperature range 25-1000°C and measured a constant Bragg-Williams parameter of S=0.93 for stoichiometric Ni_3Al.

The exact mechanism by which LRO develops has not yet been fully established, but Corey and Lisowsky 1967, Corey 1970 and Corey, Rosenblum and Green 1973 have proposed that the reaction is continuous and thermodynamically of second order. Corey et al 1967, 1973 have also suggested that, within the miscibilty gap, ordering precedes phase separation. It may be noted that this sequence of reactions is consistent with a second order, order-disorder transition, followed by a first order spinodal transformation.

Among studies of short range order are those by

Hornbogen and Kreye 1966 ; Corey, Rosenblum and Greene

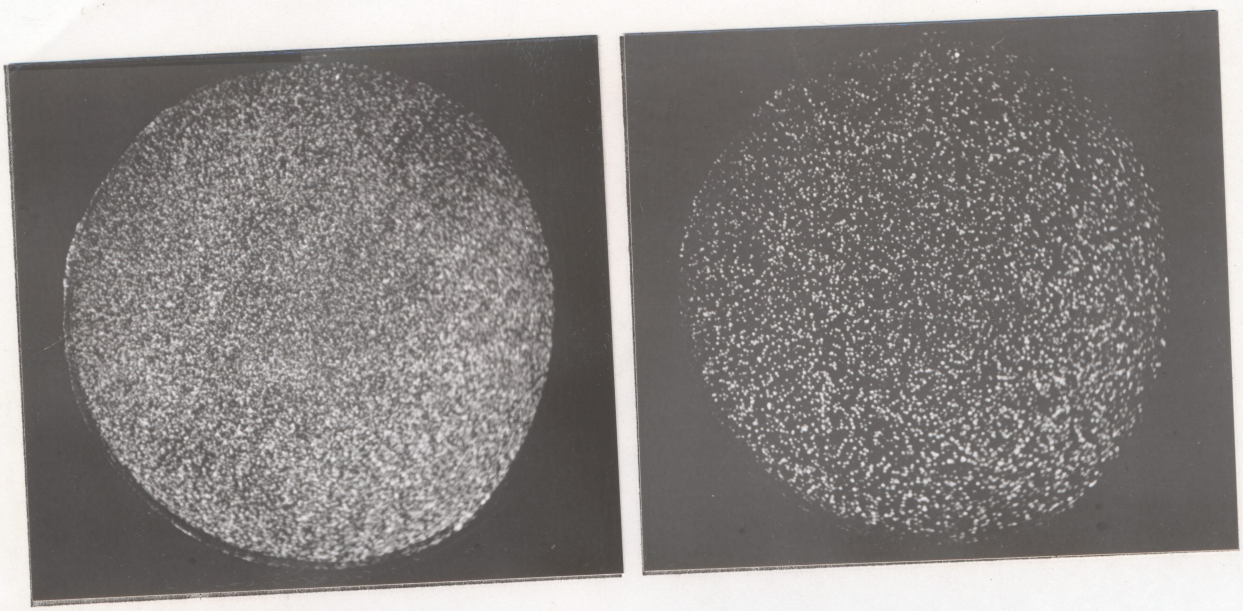

a)

b)

c)

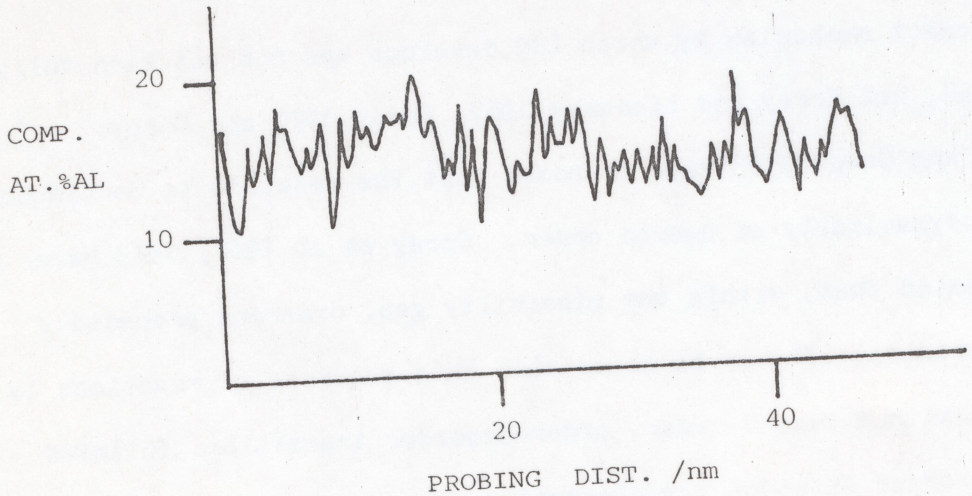

Figure 4.2 APFIM analyses of melt-spun material:- a) IAP image from Ni^{2+}, b) Al^{2+}, c) QAP composition profile.

1973 and Starke, Gerold and Guy 1975.

4.2.3 Coarsening

Ardell and Nicholson 1966, Ardell, Nicholson and Eshelby 1966 and Ardell [1968, 1972] (for example) have shown that coarsening of the γ' in nickel-aluminium alloys obeys a VDC, $t^{1/3}$ law extremely closely, with no correction for volume fraction. Alignment of γ' particles (e.g. see also Tyapkin, Travina and Ugarova 1979) has been discussed in Chapter 1 above.

4.2.4 Summary

Previous work has led to suggestions of both conventional nucleation and spinodal decomposition in this system. The evidence suggests that the latter is favoured at high supersaturations, but considerable controversy still exists in the literature.

The aim of the present study is to produce further experimental evidence with which the remaining difficulties may be resolved.

4.3 Results

4.3.1 Atom- Probe Microscopy

4.3.1i Quenched alloy

A melt-spun alloy exhibited no apparent inhomogeneities. Qualititatively, IAP analyses showed uniform distributions of nickel and aluminium (figures 4.2a and 4.2b) and QAP traces of composition versus distance exhibited only small, random fluctuations in composition (figure 4.2c). This result was checked quantitatively by analysis of QAP traces according to the χ^2 test. All χ^2 values

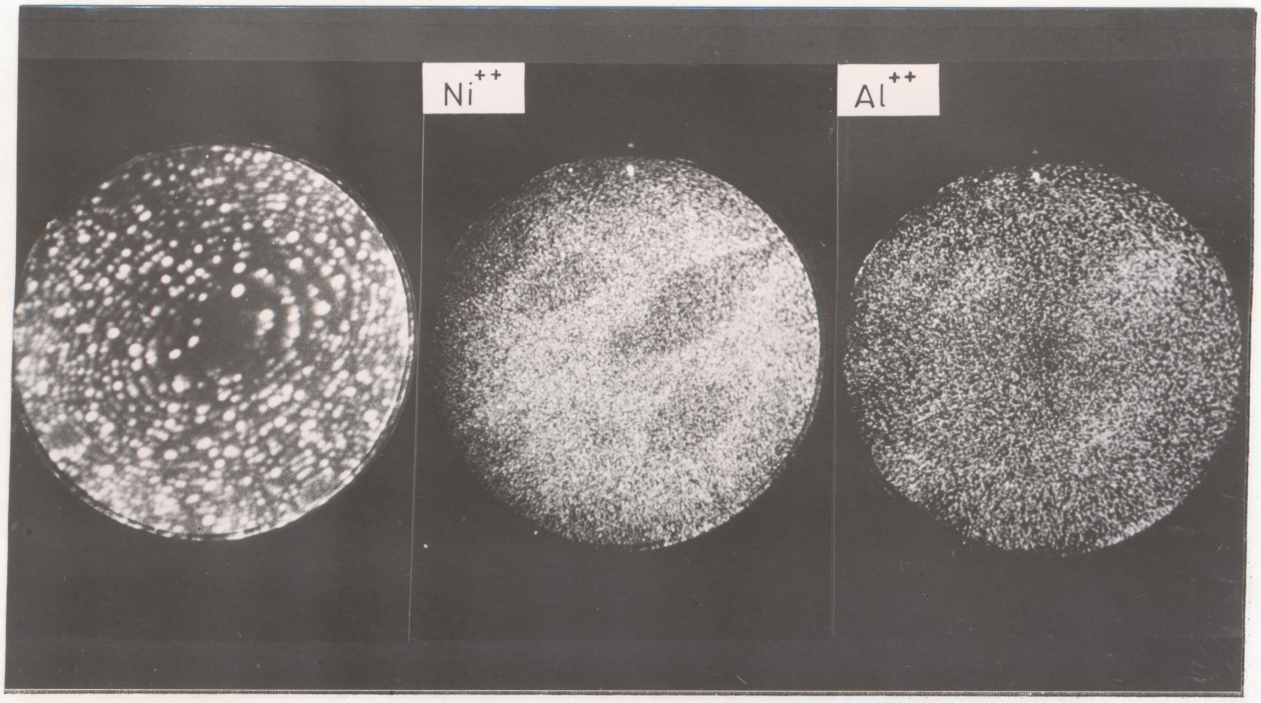

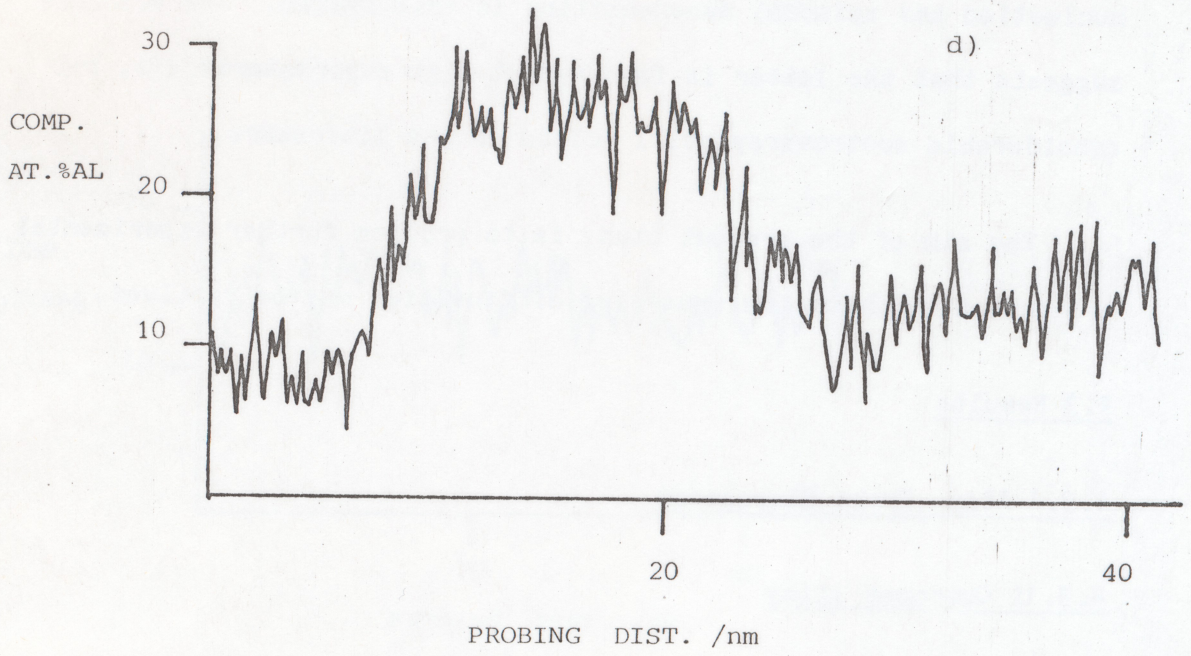

Figure 4.3 APFIM analyses of water-quenched material (two-phase):-
a) FIM image, b) IAP image from Ni^{2+}, c) Al^{2+}, d) QAP composition trace.

obtained from various data chains showed (upon comparison with contingency tables (e.g. Pugh and Winslow 1966)) a 50-95% probability that the tested data obeyed a true normal distribution. APFIM specimens quenched rapidly from solution treatment temperature into iced brine displayed a few inhomogeneities; decomposition to γ / γ' microstructure was by no means general, but some composition modulations outside 3σ from the mean were noted and a very few scattered well-defined second-phase particles were found. As the quench rate was reduced still further, however, (slow transfer to water), precipitation on a scale of ~10 nm was observed. This is illustrated in figure 4.3 which presents IAP micrographs taken from a water-quenched specimen. The Ni^{2+} (figure 4.3b) and Al^{2+} (figure 4.3c) images show two phases; one aluminium-rich and one nickel-rich. Inspection of the corresponding field-ion image (figure 4.3a) reveals a pattern of alternating bright and dim rings in the aluminium-rich regions (i.e. an ordered region e.g. Taunt and Ralph 1974). QAP analyses of these regions showed an aluminium content of 25at.% (figure 4.3d).

On the basis of these observations of phase separation only the rapid brine-quenched alloy was employed for subsequent studies of γ' generation.

The overall aluminium content of the alloy, determined by summation over all traces from rapidly quenched material, was 14.1at.%. This was in good agreement with an independent wet chemical

a)

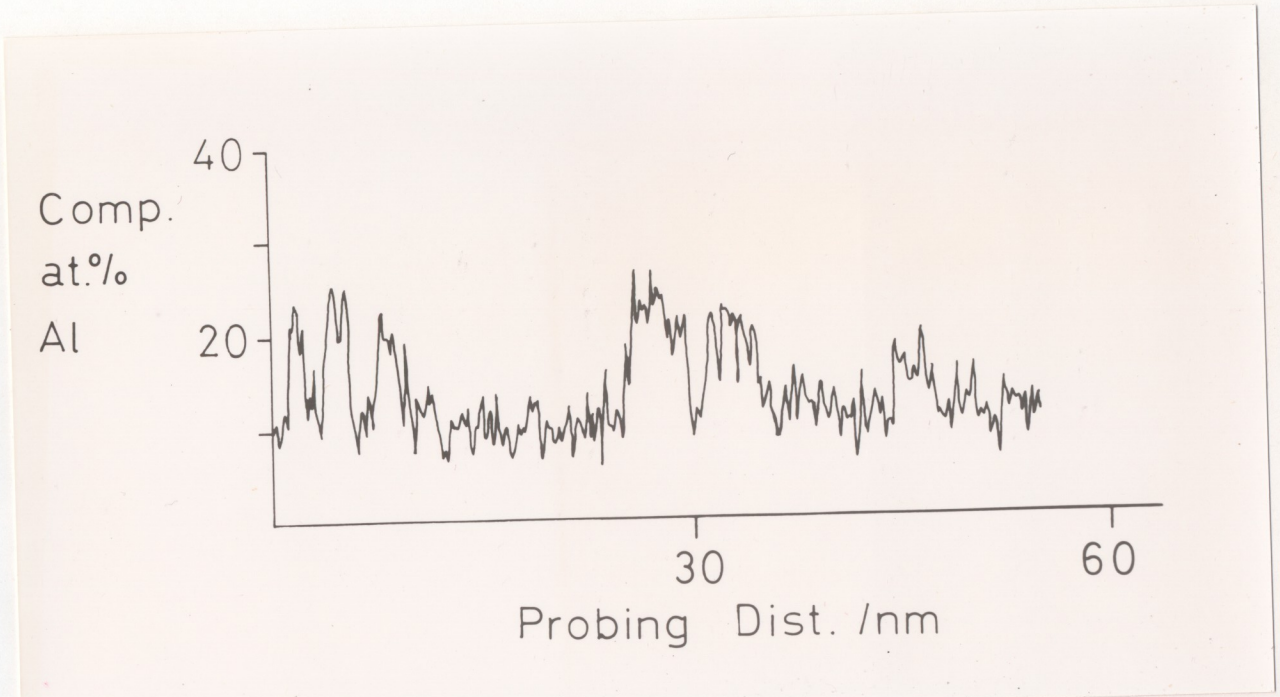

b)

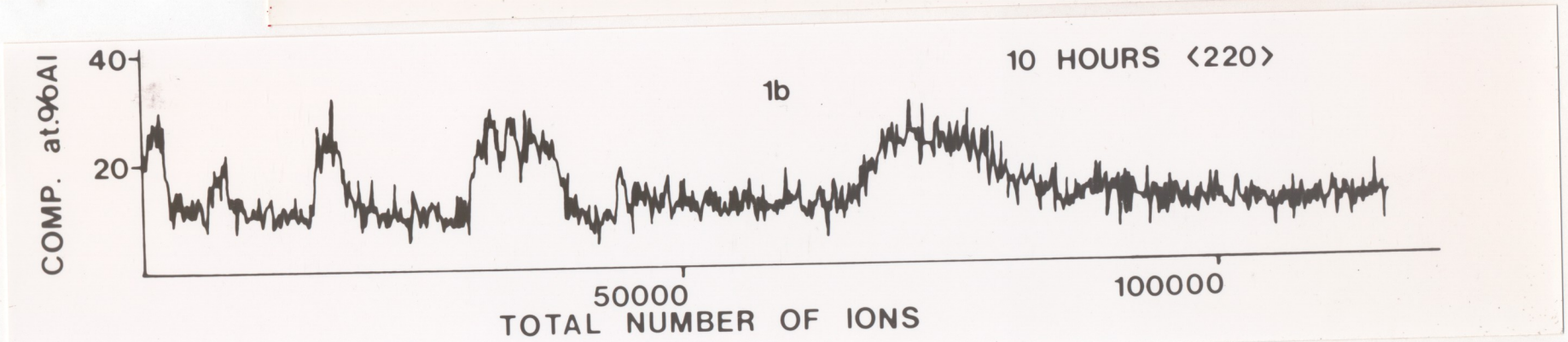

Figure 4.4 Composition profiles from alloy aged a) 0.5 hours and b) 10 hours.

~150nm

analysis of 14at.%Al.

4.3.1ii Aged alloy: qualitative results.

The generation of γ' phase was studied both qualitatively and quantitatively as a function of ageing at 625°C for periods ranging from 0.5-1000.0 hours. Two QAP traces from material treated for 5 hours and 50 hours (probing direction <111>) have already been presented in figure 3.6. Figure 4.4 shows two further composition profiles from alloy aged 0.5 hours (a) and 10 hours (b), with probing direction <110>. All of these traces, and those from other heat treatments, show separation of an aluminium-rich phase within a nickel-enriched matrix.

After only 0.5 hours ageing some precipitates had attained a mean composition of 25at.% aluminium but several others showed lower contents of 21-23at.% (e.g. figure 4.4a). As ageing time increased fewer particles of content below 25at.% aluminium were noted, with formation of the approximately stoichiometric phase apparently complete after 10 hours. Thereafter the well-defined particles (see TEM, section 4.3.2 below) apparently coarsened, maintaining a composition amplitude of 25at.%.

Approximate particle sizes were measured as 10 nm for the first few hours of ageing (up to 10 hours) followed by increase to ~250nm by 1000 hours.

4.3.1iii Aged alloy: quantitative studies.

QAP traces were also analysed by the Discrete Fast Fourier Transform method described in Chapter 3. The growth of dominant

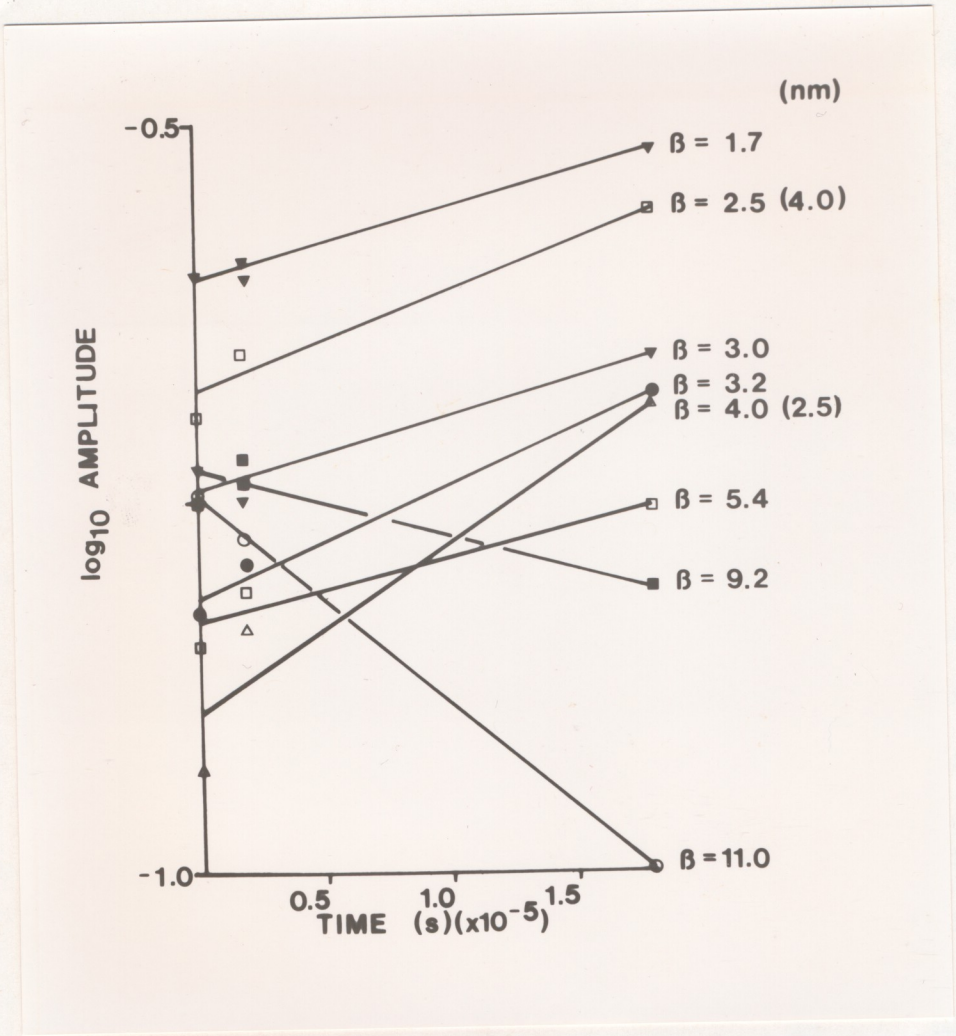

Figure 4.5 Change in amplitude of selected Fourier wavenumbers, β, with time, t, (<111>).

a)

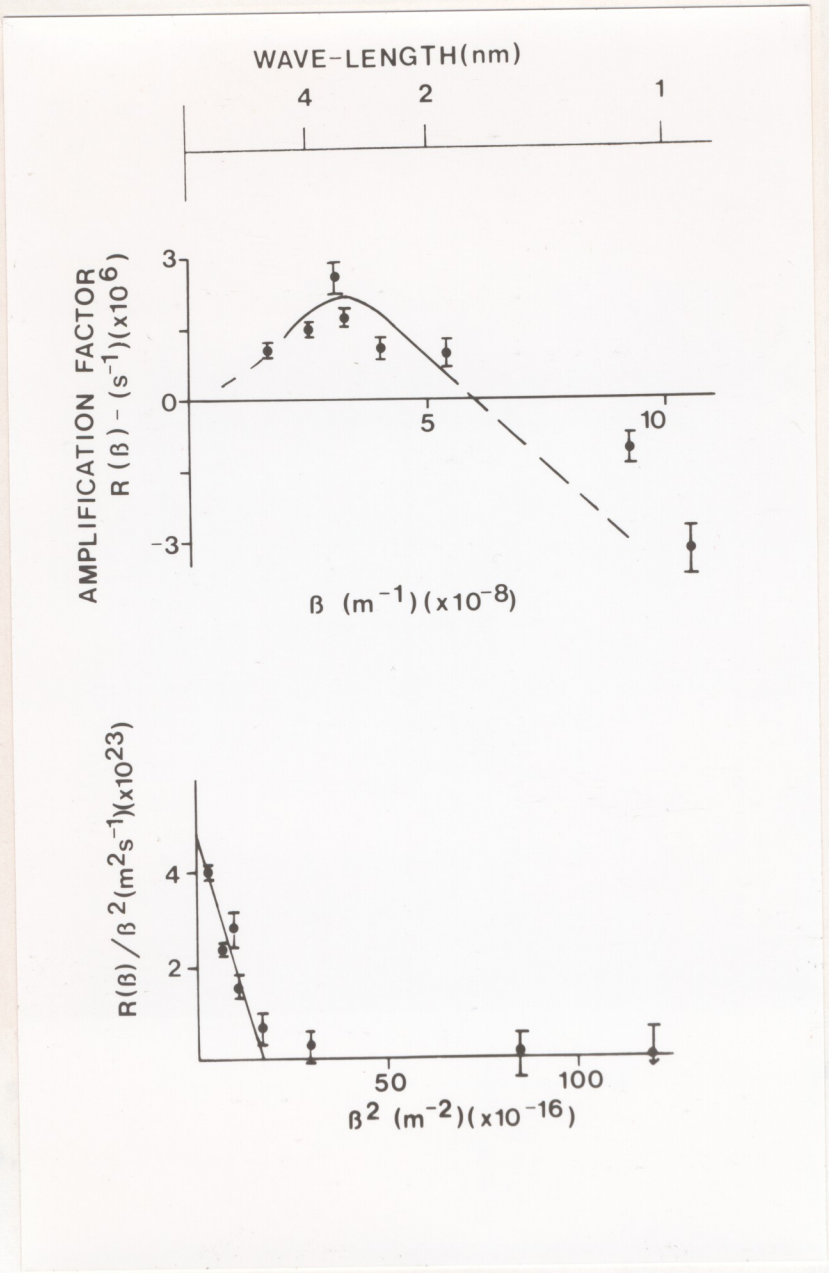

Figure 4.6 Plots of R(β) vs. β (a) and R(β)/β^2 vs. β^2 (b) for ⟨111⟩ probing direction.

wavelengths in the resulting Fourier spectra was followed as a function of ageing time, and used to examine the relationships $R(\beta)$ versus β and $R(\beta)/\beta^2$ versus β^2 which have characteristic forms for spinodal changes (see Chapter 2). $R(\beta)$ is the amplitude factor of Fourier wavenumber β. Two sets of analyses were performed for separate probing directions <111> and <110>.

4.3.1iii(a) <111> probing direction.

Two examples of final Fourier transforms for <111>-oriented specimens have already been shown in figure 3.8. Certain dominant wavenumbers are apparent (e.g. $\beta=2.5\times10^{+8}m^{-1}$). The change in amplitude with ageing time of Fourier wavenumbers β is shown in figure 4.5. For small β the gradient is positive, changing to negative as β is increased.

The numerical gradients, $R(\beta)$, derived by assuming that amplitude change is linear with time, are shown plotted against β in figure 4.6a. It may be seen that, in the region of small β, $R(\beta)$ reaches a positive maximum at $\beta=3\times10^{+8}m^{-1}$ or ~35nm. The slopes then fall towards a cut-off at $\beta=6\times10^{+8}m^{-1}$.

The plot of $R(\beta)/\beta^2$ against β^2 is shown in figure 4.6b. At small β^2 values an approximately linear relationship is obeyed, with a negative slope and positive intercept on the y-axis. As β^2 increases the graph breaks positively from linearity. Using the y-axis intercept and the equations of Chapter 2, a value of $-4\times10^{-19}m^2s^{-1}$ was obtained for the interdiffusivity, $\tilde{D}$. The value of f" was estimated

a)

b)

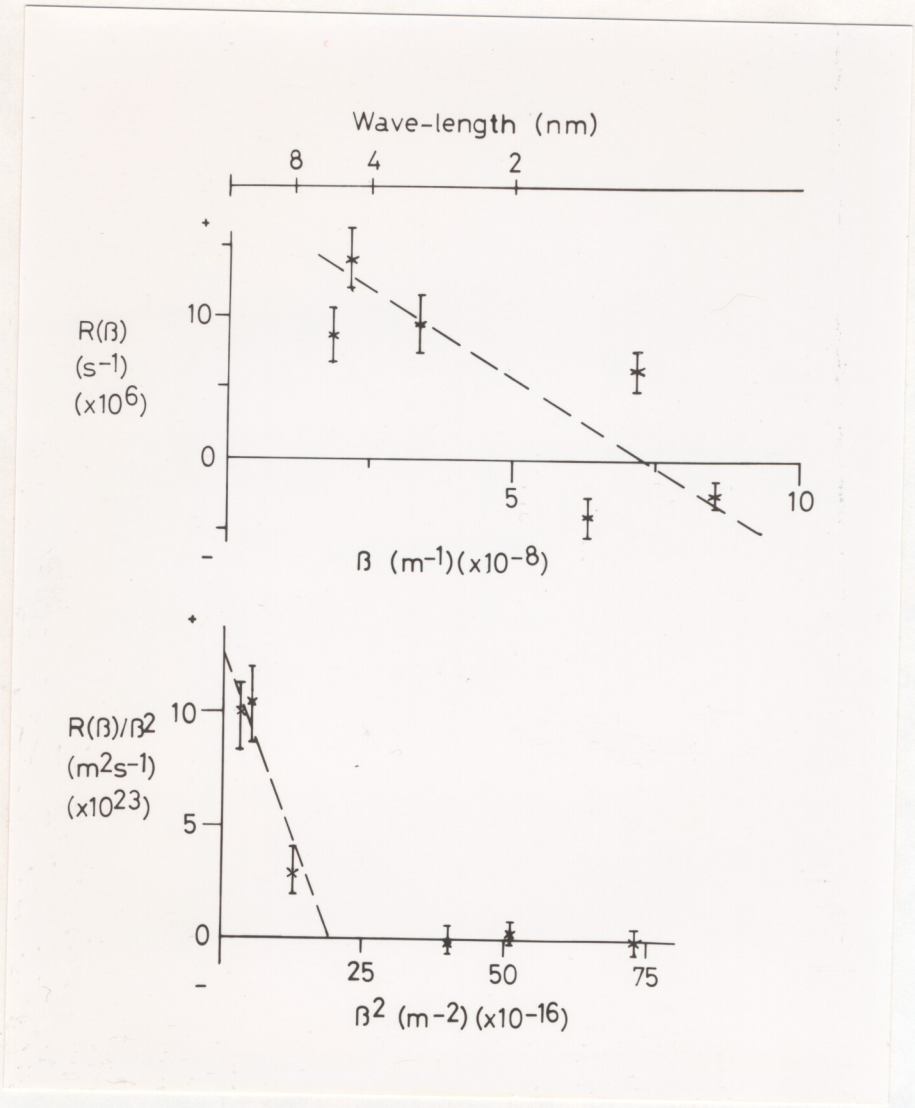

Figure 4.7 Plots of $R(\beta)$ vs. β (a) and $R(\beta)/\beta^2$ vs. β^2 (b) for <110> direction and data up to 10 hours ageing.

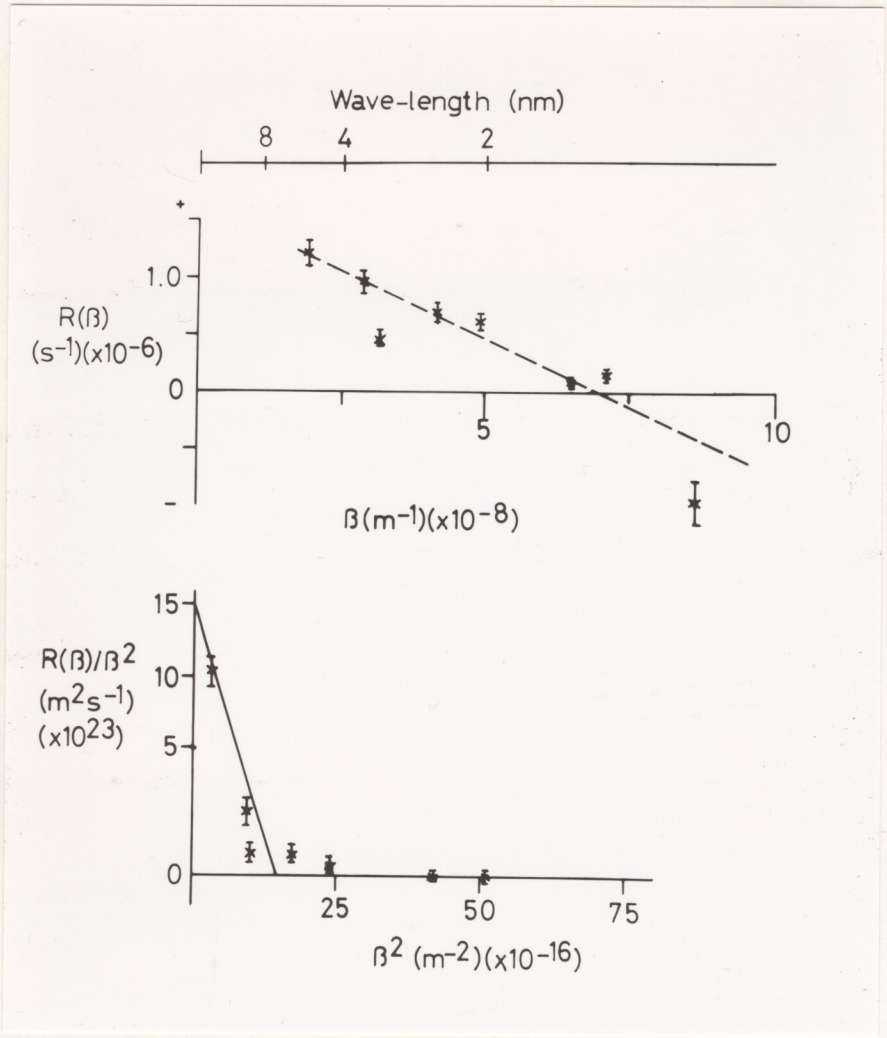

Figure 4.8 Plots of R(β) vs. β (a) and $R(\beta)/\beta^2$ vs. β^2 (b) for <110> direction and data up to 150 hours ageing.

by extrapolation of data from Hansen and Anderko 1958.

4.3.1 iii(b) <110> probing direction.

Two <110> analyses were made. The results of the first, concerning amplitude changes within only the first 10 hours of ageing, are shown in figure 4.7 ($R(\beta)$ v. β in 4.7a and $R(\beta)/(\beta^2)$ versus β^2 in 4.7b). Although less conclusive, the general trends shown by these figures resemble those of the <111> analysis, with a negative gradient and positive y-intercept for $R(\beta)/(\beta^2)$ against β^2. The reasons for greater scatter in the <110> data are discussed in section 4.4.

The second <110> analysis included data from material aged for 150 hours in order to illustrate the effect of inclusion of longer ageing times. The results (figure 4.8) are again similar to those for the <111> sequence. The major changes effected by the additional data are broadening of the $R(\beta)$ against β curve, and increasing deviation from linearity of $R(\beta)/(\beta^2)$ versus β^2.

A small and negative value for $\tilde{D}$ of $-1\times10^{-18} m^2 s^{-1}$ was estimated from the <110> sequences.

4.3.2 TEM observations.

Microstructural development throughout the ageing sequence was also followed by TEM. The observations were similar to those already reported (see section 4.2 above for a summary) with the exception of microstructures found after short ageing periods of 10 hours or less. At these early ageing times striated contrast was observed rather than discrete precipitation.

Figure 4.9a shows the structure of iced-brine quenched material.

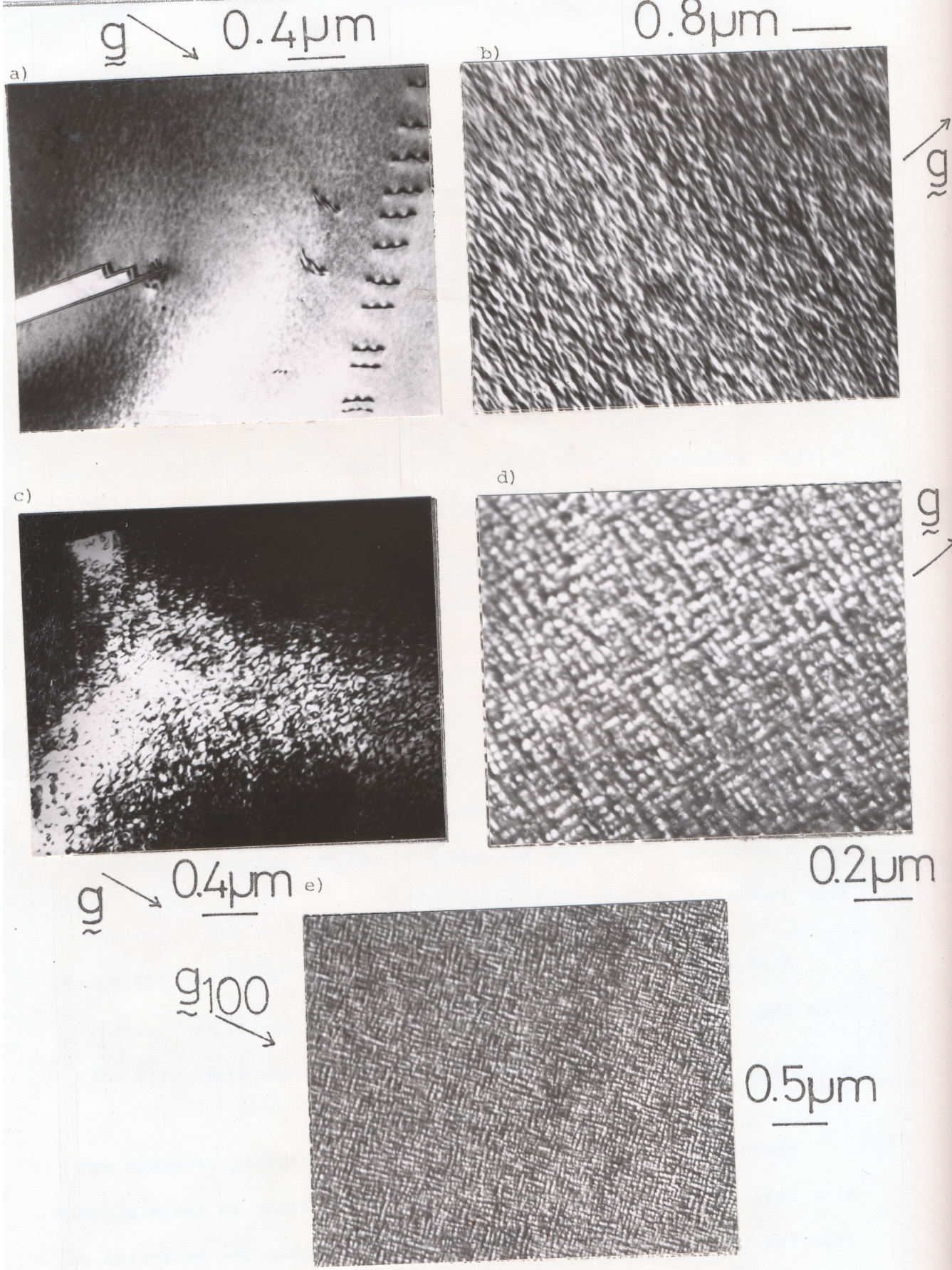

Figure 4.9 Transmission electron micrographs at various stages of ageing at 625°C:- a) as quenched b) 5 hours c) 10 hours d) 50 hours e) 150 hours.

No general and gross decomposition is evident, but mottled background contrast should be noted, particularly on bend contours. The micrograph also shows an annealing twin and sets of paired dislocations.

As the alloy was aged, development in contrast of the mottled background was observed. The resulting regularly striated structure is illustrated in figures 4.9b and 4.9c which were taken respectively after 5 hours and 10 hours at 625°C.

After 50 hours heat treatment discrete second phase particles were resolved (figure 4.9d) as expected from the literature and superlattice-centred dark-field images could be obtained. In many cases precipitates appeared to be ogdoadically diced. Alignment along <100> was noted. As ageing times increased still further the aligned microstructure coarsened (see figure 4.9e after 150 hours). A mean particle diameter of ~250nm was attained after 1000 hours. No evidence of incoherency was found.

Throughout the TEM studies of intragranular regions considerable care was taken to optimise photographic conditions under which satellites to main diffraction spots might be recorded in selected area diffraction work. No such sidebands were recorded, however.

Some studies were also made of grain-boundary regions, and a proportion of boundaries was found to exhibit cellular precipitation.

1.6μm

Figure 4.10 Cellular colonies at a grain boundary in alloy aged for 1 hour at 625°C.

Figure 4.10 shows some cellular colonies formed after 1 hour at 625°C.

4.3.3 X-ray Powder Diffraction.

X-ray diffraction data confirmed the results presented above. Sidebands corresponding to modulations of wavelength of ~8nm were recorded (Daniel and Lipson 1943; Tsujimoto, Hashimoto and Saito 1977).

4.4 Discussion

4.4.1 Atom-Probe Observations

4.4.1i Composition profiles

Statistically a 50-95% probability of true normal behaviour indicates likelihood that the data employed were randomly distributed (e.g. Yule and Kendall 1968, Loveday 1969). Such a result for the analysis of composition profiles of melt-spun alloy suggests that phase separation in the material has been suppressed. The suggestion is consistent with uniform IAP images.

In other quenched specimens some degree of phase separation is seen. Two modes are apparently operative: generation of discrete particles of second phase, and continuous composition modulation. In each case the net decomposition product contains 25at% aluminium indicating γ' formation.

Considering discrete precipitation first, only a few particles were seen in rapidly (iced-brine) quenched material but the incidence increased significantly as quench severity was reduced. The appearance of scattered phase, with a short incubation time inferred

from the behaviour of the melt-spun alloy, suggests isolated nucleation during the iced-brine quench. This is consistent with the observation of an increase in precipitate number with slower quench: more time is spent at the temperature of most probable nucleation in the latter case.

Continuous phase separation is characterised by growth in amplitude, towards stoichiometry, of initially low-amplitude composition excursions of constant wavelength. When studied by APFIM these low-amplitude compositional excursions of continuous phase separation must be distinguished from γ' regions which apparently have aluminium contents below stoichiometry (25at.%) and which arise because γ and γ' regions are sampled simultaneously. The present experimental results show a relatively high proportion of such events initially while after 10 hours ageing only a few such regions remained. The sampling effect may only account for isolated low-aluminium regions, however. Thus the decrease of incidence upon ageing indicates that at least some low-aluminium regions result from the decomposition mode. This in turn suggests that decomposition may proceed spinodally.

Coarsening of the γ/γ' microstructure is in accord with previous studies of behaviour (e.g. Ardell and Nicholson 1966).

4.4.1ii Kinetic analysis: Interpretation with respect to Cahn's theory of spinodal decomposition

The overall characteristic of spinodal reactions is a negative interdiffusivity $\tilde{D}$. In addition Cahn's theory (Chapter 2) predicts the following:

i) $R(\beta)$ versus β shows a positive maximum at small β. $R(\beta)$ then decreases towards negative values with positive cut-off at $\beta_c = \sqrt{2}\,\beta_m$.
ii) $R(\beta)/\beta^2$ versus β^2 is linear with negative gradient and positive intercept on the y-axis.

The results of <111> analyses agree substantially with these predictions (c.f. investigations of Al-Zn by e.g. Rundman and Hilliard 1967, Bartel and Rundman 1975). Two minor discrepancies arise between current data and Cahn's predictions:
i) The experimental value of β_m occurs at $0.5\beta_c$ and not $\beta_c/\sqrt{2}$ and
ii)the linear portion of figure 4.6b is only valid for $\beta < 20\times10^{-16} m^{-2}$ and not over the entire range of β.

As the experimental analysis contains some data from longer ageing sequences deviation from strict linearity is to be expected: higher terms in the diffusion equation can no longer be ignored. Also, no account has been taken of random diffusion effects or of ordering which occurs to yield the equilibrium γ' phase. These latter effects are encompassed by unified theories of continuous transitions discussed in section 4.4.1iii. Overall, however, the experimental data show reasonable agreement with Cahn's theory, suggesting that decomposition may be continuous. Certainly a small negative diffusion constant is derived.

Data for <110> analyses support this conclusion. In both cases analytical results are less complete that those for the <111> data, but the general forms of the plots obey Cahn's predictions. Comparison of the two <110> analyses clearly demonstrates further broadening of $R(\beta)$ versus β and non-linearity in $R(\beta)/\beta^2$ versus β^2 as data which are more pertinent to coarsening are included (e.g. Cahn

1966). Again the interdiffusivity is small and negative.

High frequency terms have been omitted from the <110> analyses because the effects of spinodal phase separation in this region of the spectrum may be masked by contributions from ordering modulations which are also sampled (see Chapter 3). Transforms were also rather noisy in this region. In principle plane-by-plane compositional variations associated with lattice ordering may be assessed independently and then subtracted from the transform by methods detailed in Chapter 3. However, for nickel-aluminium alloys these data are not available and cannot yet be estimated as the relative rates of ordering and spinodal changes are not known. It was thus considered most sensible to limit studies of high frequencies to <111> probing sequences where no plane-by-plane compositional change accompanies superlattice formation. The effects of ordering upon reaction kinetics are included in unified treatments of continuous transitions which are discussed below in section 4.4.1iii.

The numerical values of diffusion constant are only very approximate as extrapolation of high temperature data is highly unreliable. However, $\tilde{D}$ values of approximately $4 \times 10^{-19} m^2 s^{-1}$ are of the expected order of magnitude (e.g. Hilliard 1970).

4.4.1iii Kinetic analysis: interpretation with respect to unified theories of continuous transitions.

Precise interpretation of experimental data is extremely difficult using the Cahn theory as account cannot be taken of the effect of ordering upon kinetics. This restriction is removed by unified transition theories. Developments of unified theories are

followed in Chapter 2. Of particular relevance to the present study are the predictions of the Cook, de Fontaine and Hilliard theory (1969) that i) the spinodal $\beta_m : \beta_c$ ratio is reduced from $1/\sqrt{2}$ to 0.5 and ii) the $R(\beta)/\beta^2$ versus β^2 plot breaks positively from linearity.

Both of these effects are observed in the present study (see also Acuña and Bonfiglioli 1974) and it seems reasonable to propose that continuous ordering may occur in the experimental alloy. It may also be noted that, subject to reduction of aliasing errors discussed in Chapter 3, more higher frequency terms may be valid for unified theory analyses than for the Cahn model. It was not considered that sufficient statistical significance could be attached to high frequency members of present transforms to justify their inclusion in kinetic analysis. However, the approach may be borne in mind for subsequent analyses.

4.4.2 TEM Observations.

The present observation of <100> striated contrast at short ageing times implies that there is a periodic variation in net matrix strain in the decomposing alloy (e.g. Armitage, Kelly and Nutting 1962; Laughlin, Sinclair and Tanner 1980). In the cubic-cubic phase transformation which occurs in the γ/γ' nickel-aluminium alloys this strain may arise either from periodic lattice parameter variations which accompany spinodal decomposition, or from continuous ordering. The ordering reaction alone cannot account for the observed scale of this structure: longer wavelength events are required. Thus the modulated contrast is probably indicative of either simple spinodal clustering or of spinodal ordering.

Similar observations of striated contrast were made by Laughlin

1976 and Watts and Ralph 1977 for isostructural Ni-14at%Ti alloy. Watts and Ralph also concluded that both ordering and phase separation may contribute to the contrast.

Tanner and Laughlin (1975) have suggested that increase in striated contrast at constant wavelength may be directly used as evidence of spinodal clustering and spinodal ordering. Such observations are certainly consistent with the operation of spinodal clustering and ordering mechanisms. However, it should be noted that this criterion alone is not sufficient to identify the transition mechanisms (see Moreen, Taggart and Polonis 1975).

Detailed examination of the early-stage striated structure suggested a slightly larger scale of low-contrast structure in quenched specimens than in those which had been subsequently aged. This may occur if isolated conventional nucleation events replace continuous decomposition during the quench (see lower quench-rate results, section 4.4.1i above), followed by isothermal reaction. Similar observations were made by Sinclair, Leake and Ralph 1974 in their study of Ni-14at%Ti alloy.

TEM observations of material aged for 50 hours or more were consistent with results published in the literature and also with the predictions of Cahn (e.g. Cahn 1966).

Although strong superlattice reflections were obtained after 50 hours, selected area diffraction work did not provide observations of the initial appearance of the ordered lattice. It is thus not possible to assign a transformation sequence to the ordering and spinodal (or spinodal ordering) reactions.

4.4.3 X-ray Observations

The results of the X-ray diffraction work were in good accord with detailed studies by other workers (e.g. Manenc 1957[a,b], 1959 and Bagariatskii and Tyapkin 1957, 1960). Those sidebands which were observed indicate only modulated microstructure and not specifically continuous change. However, their occurrence is a feature of spinodal phase separation. Overall, therefore, experimental results suggest that decomposition proceeds by spinodal reaction.

4.4.4 The Overall Phase Transformation

4.4.4i Transitions identified

Two major transitions have been identified in the model alloy: spinodal phase separation (supporting Gentry and Fine 1972, Corey, Rosenblum and Greene 1973) and an order-disorder transition (Corey and Lisowsky 1967, etc.) In addition some nucleation (e.g. Kirkwood 1970, etc.) was noted during slower quenches and a cellular reaction (Williams 1959) was found at grain boundaries.

It was observed that both phase separation and ordering occur extremely rapidly and no transformation sequence could be assigned. It is also possible, however, that the reactions are coupled to give spinodal ordering.

In the case of b.c.c. Fe_3Al alloy Allen and Cahn (e.g. 1976b) have shown that uncoupled transformation steps may be separated by suitable suppression of one reaction by alloying and heat treatment. Similar suppression may be possible for f.c.c. alloys, which may provide a means of assigning phase transition sequences to f.c.c.

systems in the future. This possibilty remains to be investigated.

The transitions observed in the present experimental study are very similar to those for Ni-14at%Ti alloy. Spinodal phase separation in Ni-14.1at.%Al is somewhat faster. However, a transformation sequence cannot be assigned even by analogy as there is also confusion concerning the behaviour of the nickel-titanium system. Recent work by Watts and Ralph 1977 suggests that the spinodal reaction may precede ordering, but this remains to be established.

4.4.4ii Comparison with the phase diagram.

The approximate position of the chemical spinodal in the phase diagram may be estimated using a method due to Cook and Hilliard (1965) (an alternative is de Keijser and Meijering 1978).

Using only the critical transformation temperature the relative positions of equilibrium two phase and spinodal boundaries are calculated from

$$c_e - c_s = c_o - c_e \left(1 - 0.422(T/T_c) \right) \quad \ldots.E4.1$$

Where the equilibrium boundary is known the spinode is fixed.

For a system with lattice disregistry the coherent spinode may be found by subtraction of the appropriate mismatch term (Chapter 2) according to the equation (Hilliard 1970)

$$T_s^* - T_s = -2\eta^2 Y\, c(1 - c)/\, kN_v \quad \ldots.E4.2$$

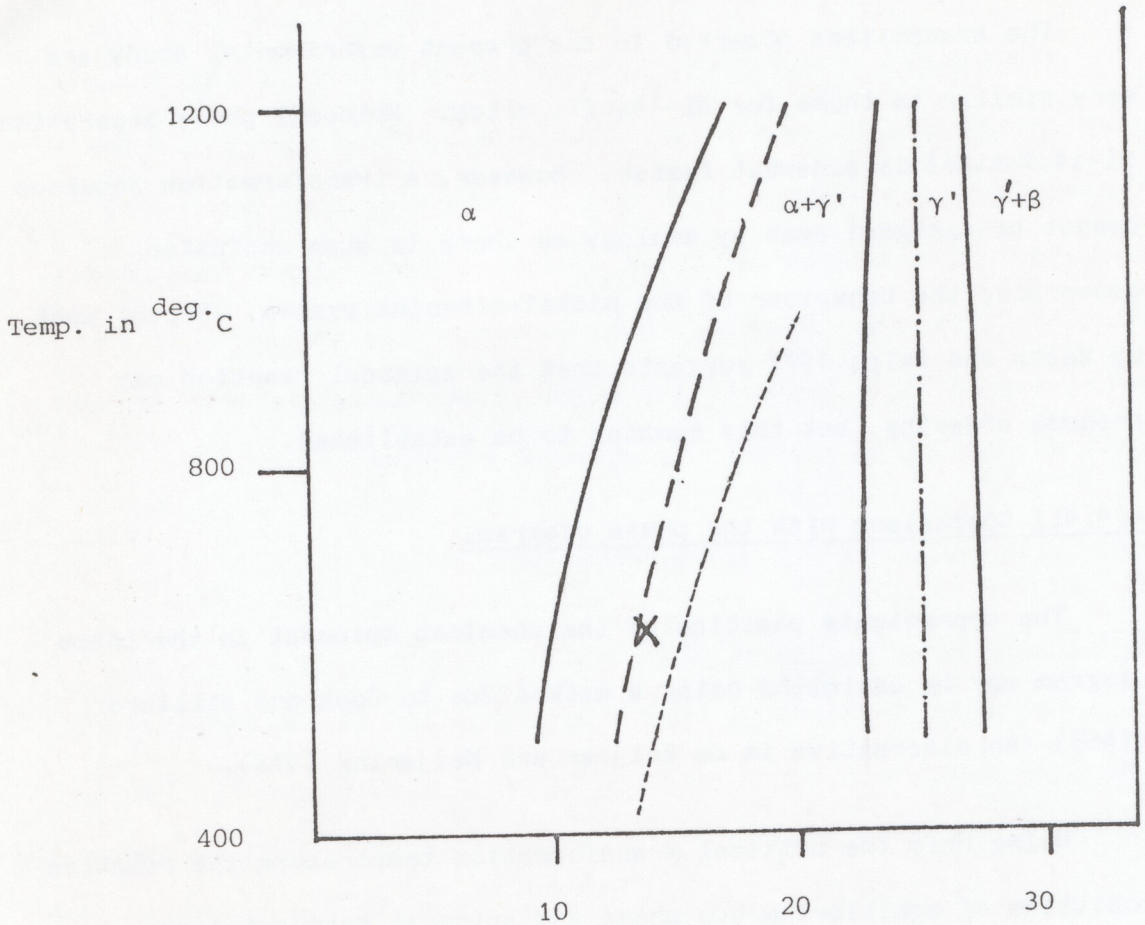

—·—·—· Ni_3Al stoichiom_etric composition

— — — estimated chemical spinodal

-------- estimated coherent spinodal

Figure 4.11 Calculated positions of coherent and incoherent spinodals in nickel-rich nickel-aluminium alloys.

The results of present calculations for the nickel-aluminium system are shown on the phase diagram of figure 4.11.

It may be seen that the experimental alloy apparently lies some way outside the coherent spinodal. Thus it has to be considered that the evidence for continuous change may indicate only continuous ordering which occurs throughout the two phase field (Chapter 2). Alternatively non-classical nucleation may be possible. However, it should be remembered that the Cook-Hilliard equation only approximates the spinodal. Also the analysis makes no allowance for compositional changes which are effected in phases due to the finite width of the γ' phase field i.e. generation of equilibrium γ' may occur at aluminium contents other than precisely 25at%. This would displace both incoherent and coherent spinodals. Thus, in the absence of evidence to the contrary, the present study indicates spinodal separation.

This result is in contrast to the findings of Wendt (1980) in a recent study of Ni-14at.%Al alloy. Wendt claimed to find no decisive evidence of spinodal compositional modulation at either 650°C or 550°C. In the latter case, however (below the present ageing temperature of 625°C), Wendt observed a plateau in precipitate size before coarsening. A similar observation was made by Sinclair, Leake and Ralph 1974 in spinodally decomposing isostructural Ni-14at%Ti alloy. As in the work of Sinclair, Leake and Ralph, the plateau observed by Wendt may be taken to be indicative of constant wavelength behaviour of some description such as spinodal decomposition i.e. certainly not nucleation and growth or coarsening. It is thus highly likely that Wendt also obtained spinodal decomposition in his work. This could possibly be identified by data reanalysis.

Overall, therefore, it is concluded that the experimental evidence indicates spinodal decomposition in Ni-14.1at.%Al at 625°C.

4.5 Summary.

This chapter has shown, using the Fourier transform analysis of Chapter 3, that phase separation in Ni-14.1at.%Al at 625°C proceeds continuously. In particular a negative diffusion constant of approximately $4 \times 10^{-19} m^2 s^{-1}$ was derived. Other major transitions observed were an order-disorder reaction and coarsening. Both ordering and spinodal decomposition proceeded rapidly and no transition sequence could be assigned. The possibility of spinodal ordering was discussed.

Nucleation of second phase was found to occur with decreasing quench rate. Also a replacement cellular phase separation reaction was identified at grain boundaries.